

Dynamical Evolution and Radiative Processes of Supernova Remnants

Stephen P. Reynolds

Abstract I outline the dynamical evolution of the shell remnants of supernovae (SNRs), from initial interaction of supernova ejecta with circumstellar material (CSM) through to the final dissolution of the remnant into the interstellar medium (ISM). Supernova ejecta drive a blast wave through any CSM from the progenitor system; as material is swept up, a reverse shock forms in the ejecta, reheating them. This ejecta-driven phase lasts until ten or more times the ejected mass is swept up, and the remnant approaches the Sedov or self-similar evolutionary phase. The evolution to this time is approximately adiabatic. Eventually, as the blast wave slows, the remnant age approaches the cooling time for immediate post-shock gas, and the shock becomes radiative and highly compressive. Eventually the shock speed drops below the local ISM sound speed and the remnant dissipates. I then review the various processes by which remnants radiate. At early times, during the adiabatic phases, thermal X-rays and nonthermal radio, X-ray, and gamma-ray emission dominate, while optical emission is faint and confined to a few strong lines of hydrogen and perhaps helium. Once the shock is radiative, prominent optical and infrared emission is produced. Young remnants are profoundly affected by interaction with often anisotropic CSM, while even mature remnants can still show evidence of ejecta.

1 Introduction

In this review, I shall first give a brief overview of the dynamical evolution and radiative properties of SNRs. I then provide a more detailed discussion of each. I shall assume a basic familiarity with fluid dynamics, shock waves, and radiative processes, at the level of Shu (1991) and Rybicki & Lightman (1979). General physics of the interstellar medium is covered in Spitzer (1978) and Draine (2011). Subse-

North Carolina State University, Raleigh, NC 27695-8202, USA, e-mail: reynolds@ncsu.edu

quent chapters in this Section cover in more detail most of the issues raised in this review.

1.1 Evolutionary Overview

As described in previous chapters, stellar ejecta are accelerated by the emerging shock wave to speeds ranging as high as $30,000 \text{ km s}^{-1}$, but with average values of order $5,000 \text{ km s}^{-1}$ for core-collapse (CC) explosions and $10,000 \text{ km s}^{-1}$ for Type Ia events. This material may be quite anisotropic, and it initially encounters material which may have been substantially modified by the progenitor system. This **circumstellar material (CSM)** is likely also to be quite anisotropic, most likely resulting from a stellar wind which may have an azimuthal density dependence, or from interaction of the progenitor star with a binary companion. For Type Ia events, it is also possible that the immediate SN environment is almost devoid of material or containing only typical ISM.

In either case, the SN **blast wave** or **forward shock** begins to decelerate almost immediately as it moves into this surrounding CSM or ISM, heating it to X-ray emitting temperatures, with a “contact discontinuity,” across which the pressure is roughly constant, separating shocked CSM/ISM from ejecta. The rapid expansion at early stages cools the ejecta adiabatically to very low temperatures, so that even a small amount of deceleration of the blast wave results in a velocity difference that is greater than the sound speed in the cold ejecta, and a **“reverse shock”** is born, facing inward, and reheating the ejecta. In even the youngest known SNRs, this reverse shock is inferred to be present.

The evolutionary stage in which both forward and reverse shocks are present can last for hundreds to thousands of years. It is sometimes called the **“ejecta-driven”** stage. During this stage, the remnant evolution depends on the density structure in the ejecta as well as in the surrounding material. Observational signatures of this phase typically center on the identifiable presence of enhanced elemental abundances in X-ray spectra. Relative contributions from the forward and reverse shocks depend on density structure as well. However, the energy radiated is a small fraction of the kinetic energy released in the explosion, so this evolution is approximately adiabatic. The progressive deceleration of the blast wave can be conveniently described with an **“expansion parameter”** m defined by $R_s \propto t^m$, with R_s the (forward) shock radius. Undecelerated expansion with $m = 1$ almost immediately gives way to $m < 1$, and various analytic solutions exist describing subsequent evolution. However, numerical simulations demonstrate the gradual decrease in m as swept-up material comes to dominate the expansion.

For constant-density ambient material, after about ten times the ejected mass has been swept up, the value of m approaches 0.4, its value for the idealized **Sedov self-similar solution** for a point explosion in a uniform medium. (There is also a Sedov solution for expansion into a power-law density gradient $\rho \propto r^{-s}$; for $s = 2$, appropriate for a steady spherically symmetric stellar wind, m approaches

2/3. However, this situation may not often be realized in practice.) Thus both the ejecta-driven and Sedov phases can be termed adiabatic. (The ejecta-driven phase is still occasionally referred to as the “free-expansion” phase, but this is not really accurate.)

For CC remnants, a neutron star is likely to be present. If it functions as a pulsar, it can inflate a bubble of relativistic particles and magnetic field, a pulsar-wind nebula (PWN), in the remnant interior. For a young, luminous pulsar, the PWN can expand and overtake inner ejecta, driving a shock into them with possible observational consequences. However, for all but exceptional cases, the pulsar energy input is not sufficient to alter the gross evolution of the shell SNR. PWNe are the subject of a later chapter.

As the blast wave decelerates, eventually the timescale for radiative cooling of the shocked material becomes comparable to the remnant age. (Cooling is typically by UV, optical, and near-IR fine-structure transitions of astrophysically common elements such as C, O, and Fe.) This is normally for shock speeds $v_s \sim 200 \text{ km s}^{-1}$, only weakly dependent on density, with corresponding ages of order 10,000 or more years. Once cooling is important, deceleration is more rapid, though the continuing presence of hot gas in the SNR interior, where cooling times are longer, continues to operate in what is called a “pressure-driven snowplow,” with $m \sim 0.3$. If that pressure is negligible, material essentially coasts, conserving (local) momentum, with $m \rightarrow 0.25$. However, by these late stages, most remnants have been interacting with inhomogeneous ISM for some time, and are quite irregular, with properties varying substantially with position in the remnant. Densities in cooling shocks can be quite high, as the compression may be limited only by magnetic pressure, so radiative-phase remnants can be quite bright in optical emission. Eventually, shock speeds become comparable to local sound speeds and the SNR dissipates into the ISM.

1.2 Radiation Overview

At different stages, SNR radiation is dominated by different processes. After the initial SN light has declined, the rapid expansion of the ejecta cools them to very low temperatures. However, the very strong, highly supersonic blast wave heats surrounding material to X-ray-emitting temperatures. Since all the relevant astrophysical shock waves in SNRs are collisionless (gas is heated not by binary collisions among particles but by interaction with a magnetic field), the particle distribution downstream is not perfectly Maxwellian. Instead, **diffusive shock acceleration (DSA)** of a small fraction of electrons crossing the shock produces a (nearly) power-law nonthermal tail attached to the thermal peak of the electron energy distribution. The tail normally extends to relativistic energies, where electrons can radiate **synchrotron radiation** at radio wavelengths. For appropriate conditions, the synchrotron component can extend all the way to the X-ray band. Optical emission at early stages is faint. These fast shocks are called **“nonradiative;”** cooling times

of the shocked gas are initially much longer than the shock age, so relatively little radiation is produced, and the compression ratio r has the value appropriate for a strong (highly supersonic) adiabatic shock into monatomic gas, $r = 4$. However, some radiation can be detected from such shocks; if the remnant expands into neutral material, hydrogen can be excited before being ionized and radiate Lyman and Balmer-series photons. Infrared radiation at early stages is predominantly thermal radiation from dust grains heated by collisions with hot gas; the temperature of that infrared emission is a good diagnostic of plasma density.

As the blast wave decelerates, the initially weak and radiative reverse shock strengthens and becomes non-radiative. The reverse shock re-heats the ejecta that overtake it, rendering them observable in X-ray emission. SNRs in this stage primarily radiate radio synchrotron emission and thermal X-ray emission from roughly solar-abundance gas behind the blast wave and from enhanced abundances of heavy elements behind the reverse shock. Disentangling these two contributions is a significant challenge in studying ejecta-driven SNRs.

The process of collisional ionization of heavier elements in either the shocked CSM/ISM or the shocked ejecta is not instantaneous. In fact, plasmas in young SNRs are typically underionized, that is, at a lower stage of ionization than would be the case for a gas in equilibrium at the observed temperature. This non-equilibrium ionization (NEI), as it is called, means that X-ray spectra depend on a parameter $\tau \equiv \int n_e dt$, the “ionization timescale,” which controls the degree of ionization of the plasma. In a shock wave, gas with all values of τ from zero up to the shock age can emit radiation. When τ exceeds a few times $10^{12} \text{ cm}^{-3} \text{ s}$, plasma is close to collisional ionization equilibrium (CIE). For typical ambient densities of order 1 cm^{-3} , this occurs in $\sim 30,000 \text{ yr}$. The ionization state of the plasma at this stage does not affect the overall dynamics, however.

Infrared emission can be produced by radiation from collisionally heated grains in either the shocked CSM/ISM or, if dust is formed in the cool ejecta, in the post-reverse-shock region. Line emission can be detected from unshocked ejecta in regions of particularly high density. Finally, a few of the youngest remnants produce detectable emission that is not related to shocks at all, but results from the decay of radioactive ^{44}Ti into ^{44}Sc and then ^{44}Ca , with the emission of hard X-ray and gamma-ray nuclear de-excitation lines and a line at 4.1 keV from filling the vacancy resulting from the electron capture decay of ^{44}Ti to ^{44}Sc .

Once the reverse shock has disappeared and the remnant is fully in the Sedov stage, spectral signatures of enhanced-abundance ejecta may still be present in X-rays in the interior. However, the shocked CSM/ISM mass dominates the shocked ejecta and the integrated spectrum. IR continuum from heated grains can still be produced.

The onset of radiative cooling dramatically alters the spectral-energy distribution (SED) of a SNR. Now, UV, optical and IR permitted, forbidden, and fine-structure transitions produce optically bright spectra dominated in optical by low ionization stages of elements like sulfur and oxygen. In fact, for SNRs in external galaxies, a powerful method of identifying radiative-stage remnants is the ratio of [S II] $\lambda\lambda$

6717, 6731 to $H\alpha$ flux, which is very much different for a radiative shock than for photoionized H II regions. Since adiabatic-phase SNRs do not produce bright optical emission, this method does not identify them. However, most of the observable life of a SNR is spent in the later phases, so a relatively small fraction of remnants in other galaxies is overlooked. For shock velocities below 200 km/s or so, X-ray emission is now quite weak. Nonthermal radio synchrotron emission from electrons with GeV energies can persist and remains the most easily observed observational signature of SNRs. The high compression ratios characteristic of radiative shock waves will also enhance the synchrotron brightness.

Nonthermal emission at X-ray wavelengths and above can be observed in a few remnants. Sufficiently energetic relativistic electrons (and positrons, if present) can produce not only synchrotron emission up to X-rays, but inverse-Compton emission from upscattering any photon fields (cosmic microwave background and possibly any locally strong IR or optical radiation) and bremsstrahlung from interaction with thermal ions. These leptonic contributions can extend to GeV and even TeV photon energies. In addition, the shock acceleration process is expected to accelerate ions as well. While they do not directly radiate, they can inelastically scatter from thermal ions, producing charged and neutral pions (and secondary positrons and electrons). The charged pions decay eventually to electrons and positrons, but the neutral pions decay to pairs of gamma-rays once the cosmic-ray proton energies are sufficient to produce π^0 particles (around 70 MeV). This “hadronic” process is the only direct evidence for cosmic-ray ions in SNRs. See Reynolds (2008) for a review of supernova remnants with emphasis on high-energy radiative processes.

2 Dynamical Evolution

I shall now consider in more detail the dynamical evolution, dividing the discussion into the phases outlined above: Ejecta-driven, Sedov, and Radiative.

2.1 Ejecta-Driven Evolution

We can consider the “initial conditions” for supernova-remnant evolution to be the distribution of ejected material once pressure forces from the original explosion are negligible (“ballistic expansion”). This is certainly true for all but very exceptional cases after a few weeks. The density profile of expanding material is determined by the density structure of the progenitor star and its interaction with the shock wave that disrupts the star. Early 1-D hydrodynamic simulations showed that both CC (nondegenerate) and Type Ia (degenerate) progenitors produced expanding profiles roughly describable as a central region of roughly constant density and an outer region of steeply declining density following an approximately power-law density dependence, $\rho \propto r^{-n}$ with $n \sim 7$ for white dwarf progenitors and $n \sim 10 - 12$ for

CC progenitors. More extensive hydrodynamic simulations and analytic calculations have refined these numbers somewhat. Dwarkadas & Chevalier (1998) find that exponential density profiles provide better fits to simulations for Type Ia SNRs. Matzner & McKee (1999) used realistic 1D stellar progenitor models for CC events and calculated the resulting ejecta distribution after the passage of the original supernova shock wave. The steep outer power-laws are reproduced, but there is a clear density jump (corresponding to the original interface between the progenitor’s hydrogen envelope and interior) of about a factor of 3 – 10, within which the density is very roughly constant.

Of course, real supernovae are not likely to be perfectly spherical. Rotation of the progenitor is an obvious cause of asymmetry, but in addition, the fundamental explosion mechanism may be asymmetric. If the **standing accretion shock instability** (SASI; Blondin et al. 2003) or another convective instability is important for CC events, material may be primarily ejected in one direction, with a high-velocity neutron star moving off in the opposite direction. In addition to large-scale asymmetries such as these, there may be smaller-scale clumping or other irregularities. Ejecta clumps are seen ahead of the average blast-wave radius in most young, and a few older, SNRs, and high-density knots of fast-moving material with enhanced abundances are seen in Cas A (roughly 330 yr old). (See, for example, Winkler et al. 2014 for SN 1006 and Hammell & Fesen 2008 for Cas A.) Radiative knots in the interior of Kepler’s SNR (CE 1604) may be CSM, but some knots ahead of the blast wave are ejecta (Reynolds et al. 2007). As the ^{56}Ni synthesized in a CC explosion decays, its decay products will heat local material which will then expand into cooler ejecta (the “nickel bubble” effect; Li et al. 1993). The effect is enhanced if the ^{56}Ni is not uniformly distributed but in clumps instead. This effect may well produce inhomogeneities in SN ejecta that are detectable in young SNRs.

The immediate surroundings of the SN are almost certainly not uniform. A steady-state constant-velocity wind in spherical symmetry produces a $1/r^2$ density profile. For spherical power-law supernova ejecta with $\rho_e \propto r^{-n}$ encountering a surrounding medium with $\rho \propto r^{-s}$, similarity solutions exist for the shock radii and for the density and pressure profiles everywhere. Outer shock waves in such cases have values of the expansion index m intermediate between 1 and the Sedov uniform-density value of 0.4: in fact, $m = (n - 3)/(n - s)$, as long as $n > 5$ and $s < 3$ (Chevalier 1982; Nadezhin 1985). As required by the self-similarity, the ratio between forward and reverse shock radii is constant; both move out, but the reverse shock is overtaken by faster-moving ejecta. The character of the solutions is quite different depending on the outer index. For the steady wind value of $s = 2$, the density peaks at the contact discontinuity; since the pressure is roughly uniform, the temperature decreases there. For uniform ISM ($s = 0$), the density drops to zero at the contact discontinuity, and the temperature rises. The same qualitative behavior occurs for decreasing, but non-power-law, ejecta density profiles, such as the exponential profile. Figures 7 and 8 show 1-D hydrodynamic simulations of a blast wave with power-law density profile moving into a uniform medium and a steady wind. The shock radii are scaled by $t^{0.4}$ (the Sedov value). Quantities are plotted as a function of the swept-up mass in units of the ejected mass.

While the forward and reverse shocks in the ejecta-driven phase are hydrodynamically stable, the region between them is not, in general. The Rayleigh-Taylor instability of a heavy fluid supported by a light one (or, in general, if the effective gravity \mathbf{g} opposes the density gradient $\nabla\rho$, $\mathbf{g} \cdot \nabla\rho < 0$) operates as the deceleration provides an effective inward gravity, and outer less dense material decelerates denser inner material. The growth rate of this instability is maximum at the contact discontinuity. It may produce turbulence that could accelerate particles; this may explain the bright ring of radio emission seen inside the outer blast wave of Cas A.

However, the surroundings may not even be spherically symmetric. It is becoming increasingly apparent that a large fraction of supernovae occur in binary systems. All SNe Ia, of course, result from binaries, but several categories of CC event, such as SNe Ib/c and IId, seem to result from stripped cores which probably require a binary companion (Smith et al. 2011). The companion star may be near enough to decelerate ejecta, possibly producing effects detectable in remnants for hundreds of years. Even if not, mass lost from either the companion or the SN progenitor star itself is likely to be asymmetric in the immediate neighborhood, probably focused into the orbital plane in a disk wind. (See Smith 2012 for a review of mass loss in massive stars.) A SN blast wave encountering an equatorially enhanced CSM, with the whole system moving at high velocity, seems to be the picture required to explain various features of Kepler's SNR (Burkey et al. 2013).

Winds of supernova progenitor systems go through various phases. A massive OB star will have a fast wind while on the main sequence, but as a red giant is likely to produce a slow, dense wind with a much higher mass-loss rate. Thus the CSM into which the SNR expands may be highly structured. The cumulative effect of the various wind phases is generally to produce a low-density cavity or bubble (Castor, McCray, & Weaver 1975), eventually of roughly constant density except near the star if mass-loss continues. There is evidence that such cavities can be produced by both CC and Type Ia progenitor systems; the SN Ia remnant **RCW 86** is an excellent example of the latter (Williams et al. 2011). A SN blast wave can race through the low-density cavity, remaining strong but not terribly luminous, until encountering the cavity wall, where a much slower transmitted shock moves into the wall while reflected shocks reheat the bubble interior. Pre-SN wind phases, or for massive stars, episodic mass loss shortly before the SN, can result in a shell of CSM at a range of possible distances. The SNR blast wave will slow on encountering the shell, but can accelerate again after traversing it. This can result in overionized shocked plasma, with observational consequences (Yamaguchi et al. 2009).

Any structure in the ambient ISM will also affect SNR evolution. SNe Ia may be encountering such material after only a few hundred years; there is evidence that Tycho's SNR (CE 1572) is interacting with such material (Williams et al. 2013). However, the ISM near Tycho appears to have a substantial gradient in density, with densities a factor of 6 or more higher on one side than the other, in addition to smaller-scale variations. Hydrodynamic simulations of remnants expanding into a smooth density gradient show that they can remain remarkably round for hundreds or thousands of years, but that their geometric centers can depart from the true ex-

plosion location by tens of percent of the mean remnant radius, complicating any search for remaining binary companions (Dohm-Palmer & Jones 1996).

In general, while the simple spherically symmetric analytic pictures are adequate for rough categorization of SNRs, detailed descriptions of individual objects require hydrodynamical simulations, generally in two and three dimensions.

2.2 Sedov Evolution

As long as the ejecta moving through the reverse shock are part of the envelope material with a steep density profile, the ram pressure upstream (inside) the reverse shock can keep it moving outward as higher-density material arrives. However, when the roughly constant-density central ejecta reach the reverse shock, this is no longer the case, and the reverse shock will move back toward the remnant center. In 1-D analytic or numerical calculations, it reflects strongly, but in 2 and 3D (and, presumably, in reality), the reverse shock does not return exactly to the remnant center, but reverberates in a complex way for a substantial transition period. However, once all the ejecta have been shocked by the reverse shock, we may assert that the remnant is fully in the Sedov stage. Analytic solutions (Sedov 1959) describe the run of density, pressure, and temperature behind the shock. The shock radius is given by a simple analytic expression: $R_s = 1.15(E/\rho)^{1/5}t^{2/5}$, where E is the explosion energy and ρ the ambient (uniform) density. (We presume a ratio of specific heats of 5/3.)

Analytic solutions have been produced by Truelove & McKee (1999) that describe the evolution in spherical symmetry from the early ejecta-driven stage through the transition into Sedov evolution. While there are self-similar solutions for a point explosion in a medium with an arbitrary power-law density profile (Sedov 1959), in almost all cases, uniform ambient density will be the best approximation. That produces a solution in which the post-shock velocity is almost linear from zero at the center to 3/4 of the blast-wave speed just behind the shock; the density drops steeply with most of the mass within the outermost 10% of the radius; and the pressure drops slightly behind the shock, leveling out in most of the interior at about 0.3 times its post-shock value. This means the temperature rises to unphysical values at small radii; in general, the interior of a Sedov blast wave consists of very hot, low-density material.

2.3 Radiative Phase

A perfectly spherical remnant in a perfectly uniform medium would experience a sudden transition when its age reached a characteristic cooling time for the gas (which depends on its composition; initial cooling is from Fe, and, as the shock slows, from elements such as C and O). At that point, gas behind the shock would

radiate away significant amounts of energy and become much more compressible. The overall shock compression ratio would rise until some other mechanism, perhaps magnetic fields, limited further compression. Hydrodynamic simulations in one and two dimensions show that the onset of cooling is sudden, with the rapid formation of a cool dense shell subject (in 2D and 3D) to instabilities which rapidly disrupt it (Blondin et al. 1998). By this time, a typical remnant is so large that the ISM it encounters is unlikely to be uniform. Remnants may encounter strong ISM inhomogeneities, such as dense molecular clouds, or may produce “blowouts” into much less dense regions (e.g., 3C 391; Reynolds & Moffett 1993). Dense material near an SNR can serve as a target for escaping cosmic-ray ions, which can produce gamma-rays from the decay of π^0 's produced in inelastic collisions with thermal gas (e.g., W28; Aharonian et al. 2008).

Since the remnant interior has a much lower density than the outer regions, it has a much longer cooling time and that gas can remain adiabatic long after the immediate post-shock gas has cooled. It can provide significant pressure to keep the expansion parameter significantly above the value of 0.25 that characterizes purely momentum-conserving evolution (Blondin et al. 1998). Remnants in this stage are large, complex objects with typically large variations in conditions at different locations. See Fig. 6 for images of later-stage SNRs.

3 Radiative Processes

As a remnant evolves through the stages outlined above, the characteristic radiation it emits changes as well. “Prompt” X-ray and radio emission from the original supernova event, generally attributed to interaction with a CSM of decreasing density, may take years to decay away. At some point, thermal X-ray emission from the increasing volume of shock-heated gas, and synchrotron emission from a nonthermal electron distribution whose maximum energy rises with time, produce true remnant X-ray and radio emission. Only one Galactic object has been caught in this rising phase: the remnant of the most recent known Galactic supernova, G1.9+0.3, brightening at both radio and X-ray wavelengths (Carlton et al. 2011). SNR 1987A in the LMC is also brightening in both regimes (see the review “Supernova remnant from SN 1987A” in this volume).

Ejecta emission. The unshocked ejecta rapidly cool over the months after the explosion to temperatures of order 100 K. However, the ejecta are illuminated by UV and soft X-ray emission from the interaction region between the blast wave and newly formed reverse shock. This radiation can ionize elements with low ionization potentials to produce near and mid-IR fine-structure lines from species such as singly-ionized iron, argon, and neon. In Cas A, where this emission can be studied in detail, temperatures of a few thousand K and densities $\lesssim 100 \text{ cm}^{-3}$ are deduced in the unshocked ejecta, although only in the denser regions; a considerable amount of lower-density material could still be present. (See Isensee et al. 2010 for a thorough study.)

Shocked ejecta will typically be heated to X-ray-emitting temperatures, $kT \gtrsim 1$ keV. However, evidence from comparing X-ray and optical data indicates that the electron and ion temperatures are not equal in fast shocks (Itoh 1978). A shock initially randomizes electron and ion speeds, so that the preshock bulk velocity is (mostly) converted to postshock random velocity. But if ion and electron speeds are equal, proton and electron temperatures would differ by the ratio of masses. The timescale for electrons to equilibrate in temperature with one another, t_{ee} , is extremely rapid, as is the equivalent for protons, t_{ii} . These are the timescales on which Maxwellian distributions are produced (e.g., Spitzer 1978). But electron-ion **temperature equilibration** takes place on a much longer timescale, so electrons and ions can have different temperatures for times not short compared to the ages of young supernova remnants. (Once full temperature equilibration has been attained, the gas will have the temperature given by the Rankine-Hugoniot shock jump conditions, $kT_s = (3/16)\mu m_p v_s^2$, where μm_p is the mean mass per particle behind the shock.) Observationally, electron temperatures determine the ionization state of the gas, and strengths of lines, while ion temperatures can only be inferred from line widths, if Doppler broadening due to bulk motions can be removed. Typical electron temperatures deduced in young SNRs are several keV, though kT_s can be 20 keV or higher (e.g., Rakowski 2005).

The emission produced by such ejecta is a combination of bremsstrahlung continuum and line emission characteristic of the ionization state of the gas. As with electron-ion temperature equilibration, ionization is not instantaneous, and SNR plasmas are very frequently ionizing (that is, their ionization state lags behind that of an equilibrium plasma at the same temperature; Itoh 1977). Ionization is typically quite rapid up to helium-like states of common elements, though lithium-like states of iron can be present as well. So a typical SNR X-ray spectrum at CCD energy resolution ($E/\nabla E \sim 20$) is dominated by blends of helium-like triplets ($K\alpha$ lines) of O, Ne, Mg, Si, S, Ar, and Ca. (See the chapter “X-ray Emission Properties of Supernova Remnants” in this volume.) In SNe Ia, L-shell transitions of Fe tend to produce a broad peak around 1 keV. Grating or microcalorimeter energy resolution ($E/\nabla E \gtrsim 100$) is required to resolve these triplets. Since ejecta contain much higher proportions of heavier elements, those line complexes are normally substantially stronger than the continuum, as compared with solar-abundance plasma.

Temperatures in the keV range are reached for ejecta densities of order 1 cm^{-3} . If clumps are present, such as the “FMK’s” (fast-moving knots) seen in Cas A, the densities can be very much higher – high enough that the shocks driven into clumps may have speeds down to a few km s^{-1} . Such a shock will be radiative, and the resulting clump emission can be primarily observed in forbidden lines of ions such as O^+ and O^{+2} . Post-shock densities in such clumps can be 10^3 cm^{-3} or greater (Peimbert & van den Bergh 1970).

If dust is formed in the cold unshocked ejecta, it can be radiatively heated by the local UV photon field, or more likely, collisionally heated once it passes through the reverse shock (e.g., Dwek & Arendt 1992). Dust in unshocked ejecta has been detected in a few cases; since the temperatures are only a few tens of K, this radiation is in the far-IR. The *Herschel* mission has found evidence for cold dust in a few

SNRs (e.g., SNR 1987A: Matsuura et al. 2011). However, in most cases, the infrared continuum one expects for ejecta dust heated in the reverse shock is not present, and limits can be set on the mass of dust produced in the SN and surviving the passage of the reverse shock (e.g., Gomez et al. 2012).

Blast wave emission. The forward shock also heats surrounding CSM or ISM to comparable temperatures, normally somewhat higher than in the reverse shock. Here too, the issues of incomplete temperature or ionization equilibrium are important. A typical pre-Sedov SNR will show a thermal X-ray spectrum which is a complex mix of blast-wave and reverse-shock emission, with varying temperatures. Decomposing that complex spectrum into the constituent parts is a demanding task.

For a CC remnant, the blast wave normally encounters ionized material. For a red supergiant (RSG) progenitor, the pre-explosion spectrum includes relatively little ionizing radiation, but the shock breakout of the RSG envelope will produce a UV flash that can ionize all the surrounding material (normally the RSG wind) out to a distance that can be many pc. A compact progenitor that has lost most of its envelope would not produce such a UV flash, but would have had a much stronger pre-explosion ionizing flux (Reynolds et al. 2007).

In contrast, all Type Ia SNRs less than a few thousand years old show emission from nonradiative or **Balmer-dominated shocks**, resulting from partially neutral upstream gas (Heng 2010). Neutral H atoms do not feel the magnetically mediated collisionless shock and remain at rest as the shock sweeps over them. On being suddenly immersed in $\sim 10^7$ K plasma, most are immediately collisionally ionized, but a few are first excited and can emit Balmer-series photons before being ionized. Those photons show a Doppler broadening reflective of the (cold) pre-shock distribution, resulting in a narrow line. Some H atoms are ionized by charge exchange, resulting in a fast neutral atom which can also emit Balmer photons, but with a velocity distribution characteristic of the downstream proton distribution, resulting in a broad line. The relative strengths, widths, and centroids of broad and narrow components of lines from nonradiative shocks contain a great deal of information about the upstream neutral fraction, the shock geometry, and the up and downstream temperatures. See Heng (2010) for a review. For young remnants, the presence of nonradiative, Balmer-dominated shocks is strong evidence in favor of a Type Ia origin. (See the chapters “Supernova/supernova remnant connection” and “Supernova remnants as clues of supernova progenitors” for more information on typing SNe from their remnants.)

SNR blast waves are virtually always easily detectable by their synchrotron radio emission. For the typical magnetic fields of tens to hundreds of microGauss, this requires electron energies of order 1 – 10 GeV; electrons radiating their peak synchrotron energy at frequency ν have energies $E = 14.7(\nu_{\text{GHz}}/B_{\mu\text{G}})^{1/2}$ GeV. For most remnants, ongoing electron acceleration is required; the interstellar cosmic-ray electron energy spectrum is considerably flatter than what is seen in SNRs, and for young remnants with adiabatic shock waves in particular, the limited shock compression means that compressing ambient magnetic field and electrons cannot produce the observed radio surface brightnesses typical of young remnants (Reynolds 2008). The radio spectra are well described by power-laws, $S_\nu \propto \nu^{-\alpha}$

with $\alpha \sim 0.4 - 0.7$ for most objects. Young SNRs tend to have steeper radio spectra; Cas A has $\alpha = 0.77$. See Green (2014) for an extensive compilation of observations of 294 Galactic SNRs.

The theory of diffusive shock acceleration (DSA) is generally thought to be responsible for the relativistic particle populations we infer in SNRs. The review by Blandford and Eichler (1987) is still an excellent introduction. If nonthermal particles make up a small fraction of the postshock energy density (the “test-particle limit”), DSA predicts a particle spectrum $N(E) \propto E^{-s}$ with $s = 2$ in a strong shock (Mach number $\mathcal{M} \gg 1$) with compression ratio $r = 4$. The synchrotron spectrum from such a population of electrons is a power-law with $\alpha = (s - 1)/2 = 0.5$.

However, if SNRs are the source of Galactic cosmic rays, the total Galactic content of cosmic ray energy requires that of order 10% of SNR energy be put into fast particles – too large for the test-particle limit. In this case, the fast particles can modify the shock structure as they diffuse ahead of the shock, producing a gradual rather than sudden change in flow velocity, until a “viscous subshock” with a compression ratio of 2 to 3 and thickness of a few ion mean free paths heats the gas. Then if (as is likely) particle mean free paths increase with energy, more energetic particles diffuse further ahead of the shock before being scattered back, sampling a larger compression ratio and forming a locally harder spectrum. That is, the energy distribution of accelerated particles becomes concave up, steeper than the test-particle limit at low energies and flatter at high energies. This effect could produce the steeper radio spectra of young SNRs. However, the large numbers of older SNRs with $\alpha < 0.5$ are still difficult to explain. Contamination of the spectrum with optically thin thermal bremsstrahlung ($\alpha = 0.1$) at higher energies could be responsible in some cases.

The maximum energy to which particles can be accelerated depends on the shock age, magnetic field, and other properties (Reynolds 1998). The time $t_{\text{acc}}(E)$ to reach an extremely relativistic energy E , for both electrons and protons, depends on the diffusion coefficient $\kappa(E)$ and shock speed v_s , where $\kappa = \lambda_{\text{mfp}}c/3$. The mean free path λ_{mfp} is often assumed proportional to the particle gyroradius r_g , $\lambda_{\text{mfp}} = \eta r_g$, (“Bohm-like” diffusion, with $\eta = 1$ giving the “Bohm limit.”) In this case, $t_{\text{acc}} \sim \kappa(E)/v_s^2$, so fast shocks can produce much higher energies. Since $r_g = E/eB$ for relativistic particles (cgs units; e is the electronic charge), high magnetic fields also produce more rapid acceleration. For ions, radiative losses are insignificant; the limitation is basically the shock age, $t = t_{\text{acc}}$. For electrons, radiative losses due to synchrotron radiation or inverse-Compton upscattering of any local photon fields can limit the maximum energy much more severely. For synchrotron losses, $E_{\text{max}} \propto B^{-1/2}$. However, since an electron of energy E radiates its peak synchrotron power at a frequency $\nu \propto E^2B$, the peak frequency ν_{max} radiated by a distribution of shock-accelerated electrons limited by losses is independent of the magnetic-field strength B .

For young remnants with shock velocities of order 1000 km s^{-1} or greater, $h\nu_{\text{max}}$ can easily exceed 1 keV, so synchrotron radiation is produced all the way from radio to X-ray energies, with electron energies reaching 10 TeV or more (Reynolds & Chevalier 1981). Thermal emission at optical and infrared wavelengths normally swamps this contribution, although near-IR observations of Cas A have identified

a synchrotron contribution. However, in X-rays, a handful of Galactic remnants are dominated by synchrotron emission (including most notably the youngest Galactic SNR, G1.9+0.3), while all historical shell SNRs show local regions dominated by synchrotron – usually, but not always, in “thin rims” at the location of the blast wave. If the rims are thin because electrons rapidly lose energy as they advect downstream, magnetic field values of 100 μG or higher are inferred (Parizot et al. 2006).

These particle energies can result in significant photon emission above the X-ray region, at GeV and TeV energies. See Reynolds (2008) for a review. Depending on the energy density of the local radiation field, inverse-Compton scattering by the same relativistic electrons can make substantial contributions, with a minimum set by upscattering of cosmic microwave background photons (“ICMB”). In addition, mildly relativistic electrons (the same that produce radio synchrotron) can produce a nonthermal bremsstrahlung contribution. Protons and other ions ought to reach energies at least as high as electrons in DSA. Relativistic ions do not radiate significantly, but can produce pions through inelastic collisions with thermal gas, once they reach the energy threshold of about 70 MeV. The neutral pions decay to gamma-rays which can be detected. There are currently a dozen or more SNRs with detected gamma-ray emission in the Fermi LAT band (GeV) or by ground-based air-Cerenkov detectors (TeV). The question of whether the gamma-ray emission from these objects is due to leptons or hadrons is actively discussed. Hadronic domination requires substantial thermal target densities. Escaping particles ahead of the SNR blast wave may impinge on dense clouds to produce emission in some cases.

The evolution of the synchrotron radio emission from a SNR is straightforward to estimate, for various possible assumptions about the efficiency of shock acceleration and magnetic-field amplification. The synchrotron volume emissivity due to a power-law energy distribution of electrons $N(E) = KE^{-s} \text{ cm}^{-3} \text{ erg}^{-1}$ can be conveniently written $j_\nu = c_j(\alpha)KB^{1+\alpha}\nu^{-\alpha}$ (e.g., Pacholczyk 1970). Then the flux density from a spherical remnant at distance d is given by

$$S_\nu = (4\pi j_\nu) \left(\frac{R_s^3 \phi}{3d^2} \right) \quad (1)$$

where ϕ is the volume filling factor of emitting material ($\phi \sim 0.25$ for a Sedov remnant with shock compression ratio 4). If the shock puts constant fractions ϵ_B and ϵ_e of the post-shock pressure ρv_s^2 into magnetic-field energy and electron energy, respectively, and if the upper and lower bounds on the electron distribution E_h and E_l do not change, we have

$$S_\nu \propto \epsilon_B^{(1+\alpha)/2} \epsilon_e R_s^3 \rho^{(3+\alpha)/2} v_s^{3+\alpha} \propto t^{m(6+\alpha)-(3+\alpha)} \quad (2)$$

since if $R_s \propto t^m$, then $v_s \propto t^{m-1}$. This assumes constant ambient density. For a remnant with a typical value of $\alpha = 0.5$, $S_\nu \propto t^{6.5m-3.5} = t^{-0.9}$ for a Sedov remnant ($m = 0.4$), and *rises* with time for an ejecta-driven remnant with $m > 0.54$ (although the simple assumptions made here may not hold for such early times). For a remnant

encountering a steady wind with $\rho \propto r^{-2}$, we have $S_v \propto t^{4.5m-3.5}$ (still with $\alpha = 0.5$) which virtually never increases.

Other assumptions are possible. If the magnetic field is not amplified but is simply compressed from a uniform value upstream, and the ambient density is uniform, then $S_v \propto t^{5m-2}$ which is constant in the Sedov phase. The shock may accelerate all electrons with energies above some threshold which varies with shock velocity. Or efficiencies may change with time. It is not known at present which of these assumptions is correct. At this time, only the Galaxy's youngest SNR, G1.9+0.3, is brightening with time at radio frequencies (Murphy et al. 2008), while the next three youngest, Cas A, Tycho, and Kepler, are all fading, at rates between 0.2 and 0.7 % yr^{-1} (Vinyaikin 2014; Stankevich et al. 2003). (An exception is the SN(R) 1987A in the LMC, which is brightening at both radio and X-ray wavelengths (Zanardo et al. 2010; Helder et al. 2013).

For reasons still not completely clear, reverse shocks are not obvious particle accelerators. The theory of DSA has been very successful in interpreting forward-shock nonthermal emission, but there may be circumstances in which other processes, such as stochastic or turbulent acceleration, play a role. The nonthermal X-ray emission in Cas A above 20 keV (Grefenstette et al. 2015) does not appear to be associated with either the forward or reverse shocks, and is still not fully understood.

Infrared continuum emission can be produced by any dust present either in the ejecta or the ISM/CSM. Many remnants show emission in mid-IR bands such as *Spitzer's* 24 μm band which is morphologically well-correlated with radio emission, and is consistent with being produced by collisional heating of surrounding dust by the forward-shocked plasma (Borkowski et al. 2006, Williams et al. 2006). This heating process depends strongly on the plasma density and much less strongly on the plasma temperature, so IR spectra, or even two-point color temperatures, can provide powerful diagnostics of SNR densities. The results can be surprising; the symmetric circular outline of Tycho's SNR masks density variations of a factor of 6 or greater (Williams et al. 2013).

Later stages. Once the reverse shock has disappeared and all ejecta have been reheated, a spherical remnant can be well described by Sedov profiles of density and temperature. Typically by this stage, gas in the outermost 10% or so of the radius (most of the material) is dense enough that electron and ion temperatures have come into equilibration, and ionization equilibrium has been reached as well (that is, the ionization timescale $\tau \equiv \int n_e dt \gtrsim 3 \times 12 \text{ cm}^{-3} \text{ s}$). While this considerably simplifies X-ray spectral analysis, the plasma temperature still varies widely, rising from its immediate postshock value toward the interior. For the fast shocks of young remnants, single-temperature plane shocks may provide adequate descriptions in restricted bandpasses.

Structure in the surrounding medium, either modified CSM or pre-existing inhomogeneities, can result in non-monotonic evolution of the blast wave speed. If the shock breaks out of a denser region into a less dense one, rapid adiabatic cooling can leave the shocked plasma in an overionized state. Spectral diagnostics of this state, including radiative recombination continuum and line ratios inconsistent with

temperatures derived from X-ray continua, have been seen in a few SNRs, of which one of the first was the middle-aged remnant W49B (Ozawa et al. 2009).

The primary change in emission properties of an SNR at late stages is the appearance of bright optical emission as the shocks become radiative and roughly isothermal. That is, an initial jump in density of a factor of 4 at the shock is followed downstream by a much larger density increase in the “cooling layer,” where much of the shock energy is radiated. This layer can be identified by bright emission from such species as O^{+2} . Compressions can reach factors of 100 or more, so regions with densities of 10^3 cm^{-3} and higher now dominate the remnant spectrum. Shock speeds are now in the range of 100 km s^{-1} or lower; optical diagnostics of various line ratios are available to characterize the temperature and density of such regions. Radiative shocks are complex and heterogeneous, typically involving a superposition of shock speeds, but models do a fairly good job of accounting for ratios of line strengths of many species that can be observed (Cox & Raymond 1985; Innes et al. 1987).

The high compressions mean that radio emission can be quite bright as well, as even without additional electron acceleration, energy densities of ambient cosmic-ray electrons and magnetic field can be increased by large factors (van der Laan 1962). Gas densities from optical diagnostics heavily favor very dense regions that occupy relatively little volume, so are probably not typical of most of the radio-emitting volume. With shock velocities of 100 km s^{-1} or lower, ongoing particle acceleration is probably weak at best. Some tendency of the very oldest SNRs to have the flattest radio spectra may simply reflect the greater importance of thermal radio contamination (Onić 2013).

Most extragalactic SNRs are found with methods that favor large optically bright radiative remnants. (See “Surveys of Supernova Remnants and Detection Techniques” in this volume.) These objects tell us as much about the homogeneity and character of surrounding ISM as about the nature of the supernova or its progenitor system. However, since most remnants spend most of their detectable lifetimes in these stages, statistics of SNRs do not suffer terribly. Most important in the analysis of such statistics is the range of ambient densities into which a population of SNRs may be evolving. Most of the scatter in distributions of SNRs in plots such as the surface brightness-diameter (“ $\Sigma - D$ ”) relation is probably caused by variations in upstream density, making these relations unreliable at best for inferring basic information about SNR evolution.

Subsequent chapters will examine in more detail these various issues.

4 Conclusions

The traditional outline of SNR evolution from free expansion to Sedov evolution to radiative snowplow provides only a crude description of a continuous development in which ejecta immediately begin interacting with CSM, with the rapid formation of a reverse shock. Deceleration of the outer blast wave begins in a few years, so

there is no real free expansion (the expansion parameter m is less than 1 almost from the beginning, and smoothly evolves toward its Sedov value of 0.4). The details of this evolution depend on the ejecta density structure. The reverse shock eventually moves to the remnant center and reheats all ejecta, though this may not occur until many times the ejected mass has been swept up. The blast wave is a strong source of thermal X-rays and nonthermal radio emission, and for young remnants, also non-thermal X-ray and gamma-ray emission. The reverse shock produces strong thermal X-ray emission as well. Until ionization equilibrium is reached, X-ray emissivities from both shocks can be much higher than for equilibrium plasmas. Since cooling times are a strong function of density, for an older remnant encountering inhomogeneous ISM, some regions (“clumps” or “clouds”) will become radiative sooner than others, and optical emission will be dominated by small regions of very high, atypical, densities. Thus the optical luminosity of an older SNR is not a good indicator of its global evolutionary state. Thermal X-ray emission from heated ISM and ejecta can remain detectable even after much of the shock is radiative. Improving our understanding of SNRs, of the supernovae that produce them, and of the CSM and ISM with which they interact, requires more realistic descriptions of both evolution and radiation.

5 Acknowledgments

I am grateful for discussions with many colleagues over many years, among whom Roger Chevalier, Kazimierz Borkowski, John Blondin, and Roger Blandford are particularly prominent. I am pleased to acknowledge support from the National Science Foundation and National Aeronautics and Space Administration for research support over the last 30 years.

6 Cross-references

All the succeeding chapters in this Section elaborate various topics I have touched on here. The Dynamical Evolution section contains references to Chapter 7, Pulsar Wind Nebulae, Chapter 8, Supernova Remnant from SN 1987A, Chapter 9, Supernova/Supernova Remnant Connection, and Chapter 10, Supernova Remnants as Clues to Supernova Progenitors. The Radiative Evolution section is elaborated in Chapters 2 – 6: Surveys, Radio Emission, X-ray Emission, UV and Optical Emission, and Infrared Emission.

References

- Aharonian et al.(2008). Aharonian F, Akhperjanian AG, Bazer-Bachi AR, Behera B, Beilicke M, Benbow W, Berge D, Bernlöhr K, Boisson C, Bolz O, Borrel V, Braun I, Brion E, Brown A M, Bühler R, Bulik T, Büsching I, Boutelier T, Carrigan S, Chadwick P M, Chounet L-M, Clapson A C, Coignet G, Cornils R, Costamante L, Degrange B, Dickinson H J, Djannati-Ataï A, Domainko W, Drury L O-C, Dubus G, Dyks J, Egberts K, Emmanoulopoulos D, Espigat P, Farnier C, Feinstein F, Fiasson A, Förster A, Fontaine G, Fukui Y, Funk Seb, Funk S, Füßling M, Gallant Y A, Giebels B, Glicenstein J F, Glück B, Goret P, Hadjichristidis C, Hauser D, Hauser M, Heinzlmann G, Henri G, Hermann G, Hinton J A, Hoffmann A, Hofmann W, Holleran M, Hoppe S, Horns D, Jacholkowska A, de Jager O C, Kendziorra E, Kerschhaggl M, Khélifi B, Komin Nu, Kosack K, Lamanna G, Latham I J, Le Gallou R, Lemièrre A, Lemoine-Goumard M, Lenain J-P, Lohse T, Martin J M, Martineau-Huynh O, Marcowith A, Masterson C, Maurin G, McComb T J L, Moderski R, Moriguchi Y, Moulin E, de Naurois M, Nedbal D, Nolan S J, Olive J-P, Orford K J, Osborne J L, Ostrowski M, Panter M, Pedalletti G, Pelletier G, Petrucci P-O, Pita S, Pühlhofer G, Punch M, Ranchon S, Raubenheimer B C, Raue M, Rayner S M, Reimer O, Renaud M, Ripken J, Rob L, Rolland L, Rosier-Lees S, Rowell G, Rudak B, Ruppel J, Sahakian V, Santangelo A, Saugé L, Schlenker S, Schlickeiser R, Schröder R, Schwanke U, Schwarzbürg S, Schwemmer S, Shalchi A, Sol H, Spangler D, Stawarz Ł, Steenkamp R, Stegmann C, Superina G, Takeuchi T, Tam P H, Tavernet J-P, Terrier R, van Eldik C, Vasileiadis G, Venter C, Vialle J P, Vincent P, Vivier M, Völk H J, Volpe F, Wagner S J, Ward M(2008) Discovery of very high energy gamma-ray emission coincident with molecular clouds in the W 28 (G6.4-0.1) field. *A&A* 481:401 – 410
- Blandford & Eichler(1987). Blandford RD, Eichler D (1987) Particle acceleration at astrophysical shocks: A theory of cosmic ray origin. *PhysRep* 154:1 – 75
- Blondin et al.(1998). Blondin JM, Wright EB, Borkowski KJ, Reynolds SP (1998) Transition to the Radiative Phase in Supernova Remnants. *ApJ* 500:342 – 354
- Blondin, Mezzacappa, & De Marino. Blondin JM, Mezzacappa, A, DeMarino C (2003) Stability of Standing Accretion Shocks, with an Eye toward Core-Collapse Supernovae. *ApJ* 584:971 – 980
- Borkowski et al.(2015). Borkowski KJ, Reynolds SP, Roberts MSE(2015) G11.20.3: The Young Remnant of a Stripped-Envelope Supernova. *ApJ*, submitted
- Borkowski et al.(2006). Borkowski KJ, Williams B J, Reynolds SP, Blair WP, Ghavamian P, Sankrit R, Hendrick, SP, Long, KS, Raymond JC, Smith RC, Points S, Winkler PF(2006) Dust destruction in Type Ia supernova remnants in the Large Magellanic Cloud. *ApJ* 642:L141 – L144
- Burkey et al.(2013). Burkey M, Reynolds SP, Borkowski KJ, Blondin JM (2013) X-ray emission from strongly asymmetric circumstellar material in the remnant of Kepler's supernova. *ApJ* 764:63
- Carlton et al.(2011). Carlton AK, Borkowski KJ, Reynolds SP, Hwang U, Petre R, Green DA, Krishnamurthy K, Willett, R(2011) Expansion of the youngest Galactic supernova remnant G1.9+0.3. *ApJ* 737:22
- Castor et al.(1975). Castor J, McCray R, Weaver R (1975) Interstellar bubbles. *ApJ* 200:107 – 110
- Chevalier(1982). Chevalier RA (1982) Self-similar solutions for the interaction of stellar ejecta with an external medium. *ApJ* 258:790 – 797
- Cox & Raymond(1985). Cox DP, Raymond JC (1985) Preionization-dependent families of radiative shock waves. *ApJ* 298: 651 – 659
- DeLaney et al.(2014). DeLaney T, Kassim NE, Rudnick L, Perley RA (2014) The Density and Mass of Unshocked Ejecta in Cassiopeia A through Low Frequency Radio Absorption *ApJ* 785:7 (16 pp)
- Dohm-Palmer & Jones(1996). Dohm-Palmer RC, Jones TW (1996) Young Supernova Remnants in Nonuniform Media. *ApJ* 471:279:291
- Draine(2011). Draine B (2011) *Physics of the Interstellar and Intergalactic Medium*. Princeton: Princeton NJ

- Dwarkadas & Chevalier(1998). Dwarkadas VV, Chevalier RA (1998) Interaction of Type Ia Supernovae with Their Surroundings. *ApJ* 497:807–823
- Dwek & Arendt(1992). Dwek E, Arendt RG (1992) Dust-gas interactions and the infrared emission from hot astrophysical plasmas *ARA&A*30:11 – 50
- The infrared diagnostic of a dusty plasma with applications to supernova remnants. *ApJ* 322:812 – 821
- Gomez et al.(2012). Gomez HL, Clark CJR, Nozawa T, Krause O, Gomez EL, Matsuura M, Barlow M J, Besel M-A, Dunne L, Gear W. K, Hargrave P, Henning T, Ivison RJ, Sibthorpe B, Swinyard BM, Wesson R.(2012) Dust in historical Galactic Type Ia supernova remnants with Herschel. *MNRAS* 420:3557 – 3573
- Grefenstette et al.(2015). Grefenstette BW, Reynolds SP, Harrison FA, Humensky TB, Boggs SE, Fryer CL, DeLaney T, Madsen KK, Miyasaka H, Wik DR, Zoglauer A, Forster K, Kitaguchi T, Lopez L, Nynka M, Christensen FE, Craig, WW, Hailey CJ, Stern D, Zhang WW(2015) Locating the most energetic electrons in Cassiopeia A. *ApJ* 802:15 (11 pp)
- Green(2014). Green DA (2014) A catalogue of Galactic supernova remnants (2014 May version), Cavendish Laboratory, Cambridge, United Kingdom (available at "http://www.mrao.cam.ac.uk/surveys/snrs/")
- Hammell & Fesen(2008). Hammell MC, Fesen RA (2008) A catalog of outer ejecta knots in the Cassiopeia A supernova remnant. *ApJS* 179:196 – 208
- Helder et al.(2013). Helder EA, Broos PS, Dewey D, Dwek E, McCray R, Park S, Racusin JL, Zhekov SA, Burrows DN (2013) Chandra Observations of SN 1987A: The Soft X-Ray Light Curve Revisited. *ApJ* 764:11 (7 pp)
- Heng(2010). Heng K (2010) Balmer-Dominated Shocks: A Concise Review *PASA* 27:23 – 44
- Innes et al.(1987). Innes DE, Giddings JR, Falle SAEG (1987) Dynamical models of radiative shocks. III - Spectra *MNRAS* 227:1021 – 1053
- Isensee et al.(2010). Isensee K, Rudnick L, DeLaney T, Smith JD, Rho J, Reach WT, Kozasa T, Gomez H (2010) The Three-dimensional Structure of Interior Ejecta in Cassiopeia A at High Spectral Resolution. *ApJ* 700: 2059 – 2070
- Itoh(1977). Itoh H (1977) Theoretical Spectra of the Thermal X-Rays from Young Supernova Remnants. *PASJ* 29:813 – 830
- Itoh(1978). Itoh H (1978) Two-fluid blast-wave model for supernova remnants. *PASJ* 30:489 – 498
- Li et al.(1993). Li H, McCray R, Sunyaev RA (1993) Iron, Cobalt, and Nickel in SN 1987A. *ApJ* 419:824 – 836
- Matzner & McKee(1999). Matzner, C.D., McKee, C.F.: The Expulsion of Stellar Envelopes in Core-Collapse Supernovae. *ApJ* **510**, 379–403 (1999)
- Matsuura et al.(2011). Matsuura M, Dwek E, Meixner M, Otsuka M, Babler B, Barlow MJ, Roman-Duval J, Engelbracht, C, Sandstrom K, Lakićević M, van Loon JT, Sonneborn G, Clayton GC, Long KS, Lundqvist P, Nozawa T, Gordon KD, Hony S, Panuzzo P, Okumura K, Misselt KA, Montiel E, Sauvage M(2011) Herschel Detects a Massive Dust Reservoir in Supernova 1987A. *Science* 333:1258 – 1261
- Murphy et al.(2008). Murphy T, Gaensler BM, Chatterjee S (2008) A 20-yr radio light curve for the young supernova remnant G1.9+0.3. *MNRAS* 389:L23 – L27
- Nadezhin(1985). Nadezhin, DK (1985) On the initial phase of interaction between expanding stellar envelopes and surrounding medium *Ap&SpSci* 112:225 – 249
- Onić(2013). Onić D (2013) On the supernova remnants with flat radio spectra. *ApSpSci* 346:3 – 13
- Ozawa et al.(2009). Ozawa M, Koyama K, Yamaguchi H, Masai K, Tamagawa T (2009) Suzaku Discovery of the Strong Radiative Recombination Continuum of Iron from the Supernova Remnant W49B. *ApJ* 706:L71 – L75
- Pacholczyk(1970). Pacholczyk AG (1970) Radio astrophysics. Freeman, San Francisco
- Parizot et al.(2006). Parizot E, Marcowith A, Ballet J, Gallant, YA (2006) Observational constraints on energetic particle diffusion in young supernovae remnants: amplified magnetic field and maximum energy. *A&A* 453: 387 – 395

- Peimbert & van den Bergh(1970). Peimbert M, van den Bergh S (1970). Optical Studies of Casiopeia A.IV. Physical Conditions in the Gaseous Remnant. *ApJ* 167:223 – 234
- Rakowski(2005). Rakowski C (2005) Electron ion temperature equilibration at collisionless shocks in supernova remnants. *AdSpRes* 35:1017 – 1026
- Reynolds(1998). Reynolds SP (1998) Models of synchrotron X-rays from shell supernova remnants. *ApJ* 493:375 – 396
- Reynolds(2008). Reynolds SP (2008) Supernova remnants at high energy. *ARA&A* 46:89 – 126
- Reynolds & Chevalier(1981). Reynolds SP, Chevalier RA (1981) Nonthermal radiation from supernova remnants in the adiabatic phase of evolution. *ApJ* 245:912 – 919
- Reynolds & Moffett(1993). Reynolds SP, Moffett DA (1993) High-resolution radio observations of the supernova remnant 3C 391 - Possible breakout morphology. *AJ* 105:2226 – 2230
- Reynolds et al.(2007). Reynolds SP, Borkowski KJ, Hwang U, Hughes JP, Badenes C, Lamington JM, Blondin JM(2007) A deep Chandra observation of Keplers supernova remnant: a Type Ia event with circumstellar interaction. *ApJ* 668:L135 – 138
- Rybicki & Lightman(1979). Rybicki GB, Lightman AP (1979) Radiative processes in astrophysics. Wiley, New York
- Sedov(1959). Sedov LI (1959) Similarity and dimensional methods in mechanics. Academic Press, New York
- Shu(1991). Shu FH (1991) The physics of astrophysics. University Science Books, Mill Valley CA
- Smith(2014). Smith N (2014) Mass Loss: Its Effect on the Evolution and Fate of High-Mass Stars. *ARA&A* 52:487–528
- Smith et al.(2011). Smith N, Li W, Filippenko AV, Chornock R (2011) Observed fractions of core-collapse supernova types and initial masses of their single and binary progenitor stars. *MNRAS* 412:1522 – 1538
- Stankevich et al.(2003). Stankevich KS, Aslanyan AM, Ivanov VP, Martirosyan RM, Terzian Ye (2003) Evolution of the Radio Luminosities of the Tycho and Kepler Supernovae Remnants. *Astrophysics* 46:429 – 433
- Truelove & McKee(1999). Truelove JK, McKee, CF(1999) Evolution of Nonradiative Supernova Remnants. *ApJS* 120:299–326
- van der Laan(1962). van der Laan H(1962) Expanding supernova remnants and galactic radio sources. *MNRAS* 124:125 – 145
- Vinyaikin(2014). Vinyaikin EN (2014) Frequency dependence of the evolution of the radio emission of the supernova remnant Cas A. *Astr.Rep.* 58:626 – 639
- Williams et al.(2006). Williams, BJ, Borkowski, KJ, Reynolds, SP, Blair WP, Ghavamian P, Hendrick SP, Long KS, Points S, Raymond JC, Sankrit R, Smith RC, Winkler PF (2006) Dust destruction in fast shocks of core-collapse supernova remnants in the Large Magellanic Cloud. *ApJ* 652:L33 – L36
- Williams et al.(2011). Williams BJ, Blair WP, Blondin JM, Borkowski KJ, Ghavamian P, Long KS, Raymond JC, Reynolds SP, Rho J, Winkler PF(2011) RCW 86: A Type Ia supernova in a wind-blown bubble. 2011, *ApJ*, 741:96 (15 pp)
- Williams et al.(2013). Williams BJ, Borkowski KJ, Ghavamian P, Hewitt JW, Mao SA, Petre R, Reynolds SP, Blondin JM(2013) Azimuthal density variations around the rim of Tycho's supernova remnant. *ApJ* 770:129 – 139
- Winkler et al.(2014). Winkler PF, Williams BJ, Reynolds SP, Petre R, Long KS, Katsuda S, Hwang, U(2014) A high-resolution X-ray and optical study of SN 1006: asymmetric expansion and small-scale structure in a Type Ia supernova remnant. *ApJ* 781:65
- Yamaguchi et al.(2009). Yamaguchi H, Ozawa M, Koyama K, Masai K, Hiraga JS, Ozaki M, Yonetoku D(2009) Discovery of strong radiative recombination continua from the supernova remnant IC 443 with Suzaku. *ApJ* 705:L6 – L9
- Zanardo et al.(2010). Zanardo G, Staveley-Smith L., Ball L, Gaensler BM, Kesteven MJ, Manchester RN, Ng C-Y, Tzioumis AK, Potter TM (2010) Multifrequency Radio Measurements of Supernova 1987A Over 22 Years. *ApJ* 710:1515 – 1529

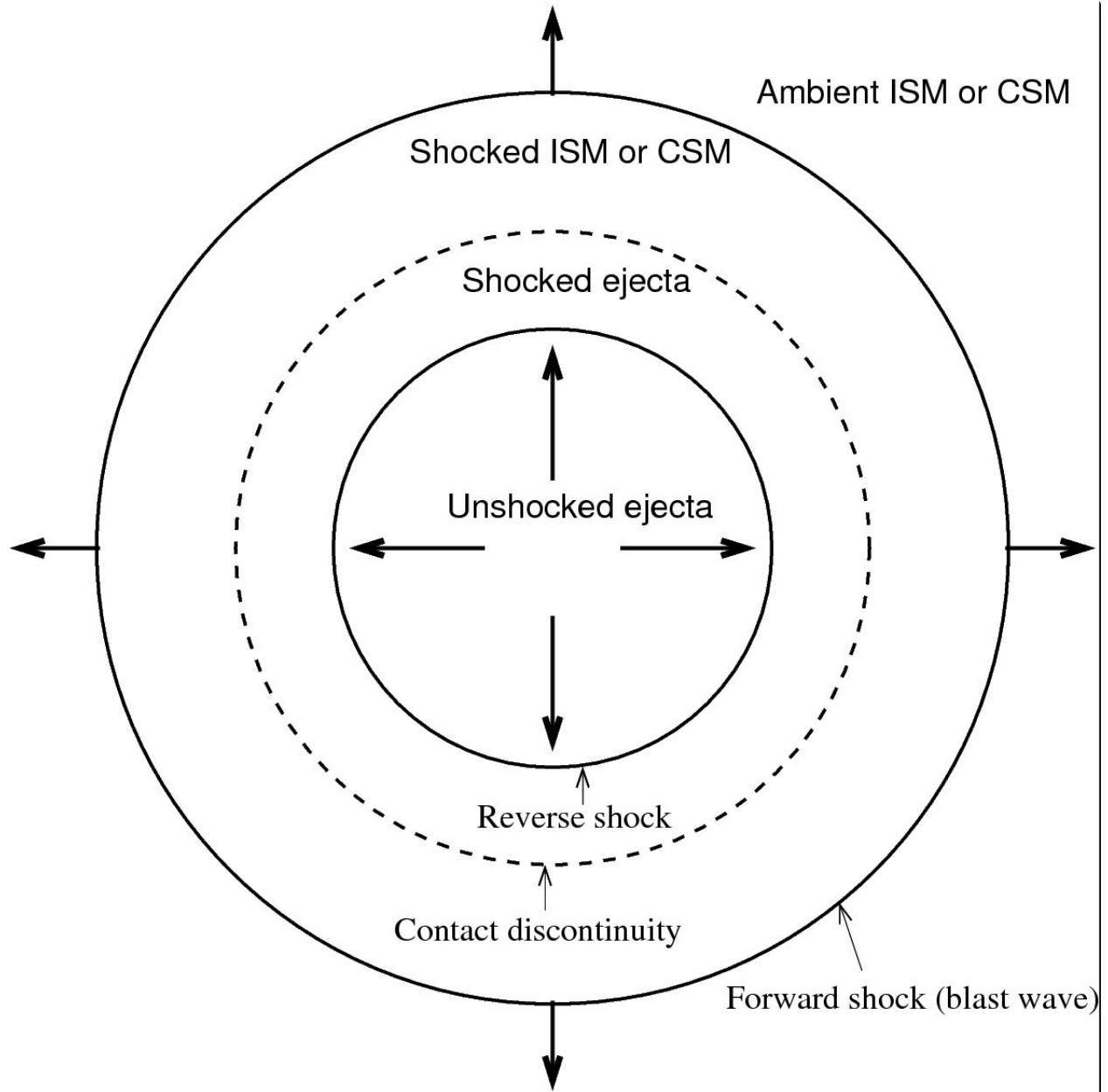


Fig. 1 Schematic of the two-shock structure of a SNR in the ejecta-driven stage. Rapidly moving, cold unshocked ejecta are heated and decelerated at the reverse shock. Hot ejecta are separated from shocked ambient material at a contact discontinuity. The forward shock or blast wave heats and accelerates ambient ISM or CSM.

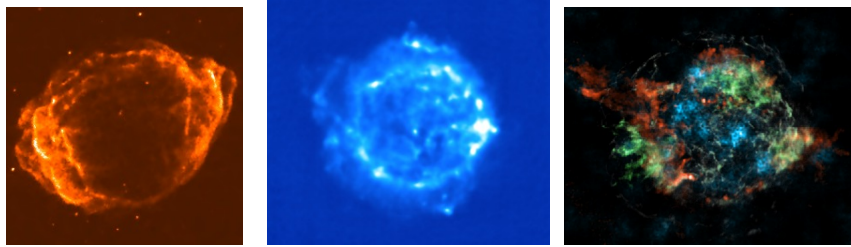


Fig. 2 Remnants of the two most recent known supernovae in the Milky Way. Left: **G1.9+0.3** (about 1900 CE) (X-rays) (K. Borkowski). Center: **Cassiopeia A** (5 GHz, VLA; DeLaney et al. 2014). Right: Cassiopeia A (about 1680 CE). Green: Si band. Red: Fe $K\alpha$ band. (both with *Chandra*; U. Hwang). Blue: ^{44}Ti emission (68 keV) with NuSTAR (Grefenstette et al. 2014).

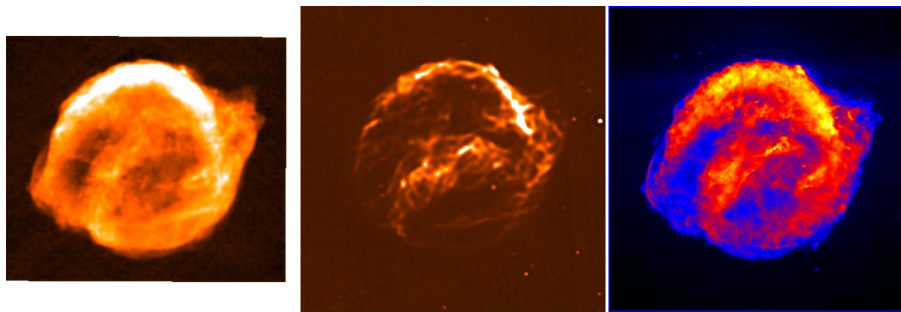


Fig. 3 The remnant of **Kepler's supernova of 1604 CE**. Left: radio (VLA at 5 GHz; T. DeLaney). Center: *Spitzer* MIPS at $24\ \mu\text{m}$ (deconvolved; K. Borkowski). Right: *Chandra* between 0.3 and 7 keV (Reynolds et al. 2007).

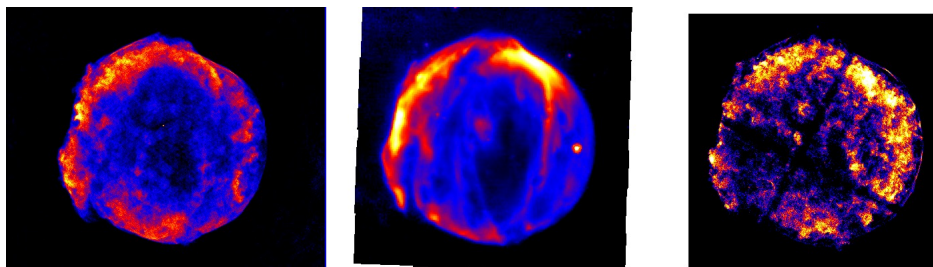


Fig. 4 The remnant of **Tycho's supernova of 1572 CE**. Left: radio (VLA at 5 GHz; Reynoso et al. 1997). Center: *Spitzer* MIPS at $24\ \mu\text{m}$ (Williams et al. 2013). Right: *Chandra* image (NASA/CXC).

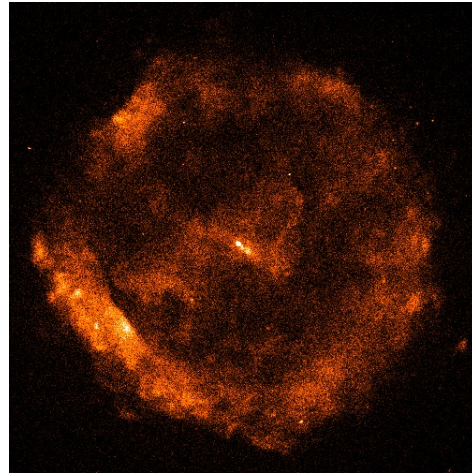
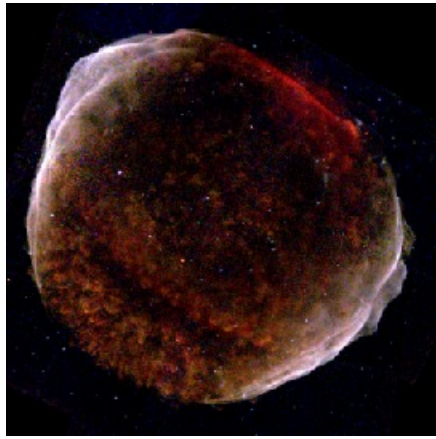


Fig. 5 Left: Remnant of **SN 1006 CE**; (X-ray, *Chandra* Winkler et al. 2014). Right: **G11.2-0.3**, roughly 2000 y old (X-ray, *Chandra*; Borkowski et al. 2015).

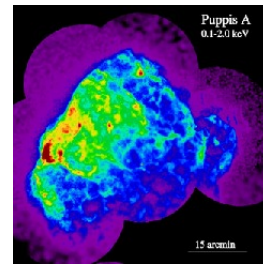
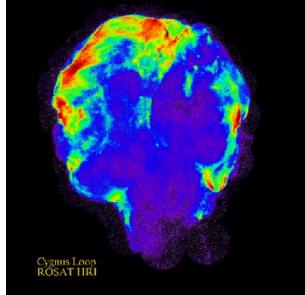


Fig. 6 Three older SNRs. Left: Three-color image of **W28**. Red: infrared; cyan: $H\alpha$; blue: radio (VLA) (NRAO/AUI/NSF; Brogan et al.) Center: **Cygnus Loop** (X-ray; ROSAT) (NASA/GSFC). Right: **Puppis A** (X-ray; ROSAT) (NASA/GSFC).

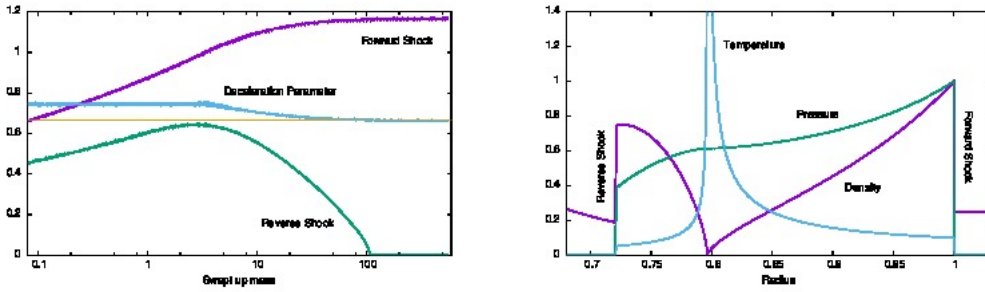


Fig. 7 Left: Shock locations and forward-shock expansion index m for the case $n = 6, s = 0$. Shock positions are scaled by $t^{0.4}$ (the Sedov value). Right: Profiles of density, temperature, and pressure during the self-similar phase for this calculation. (J. Blondin, private communication)

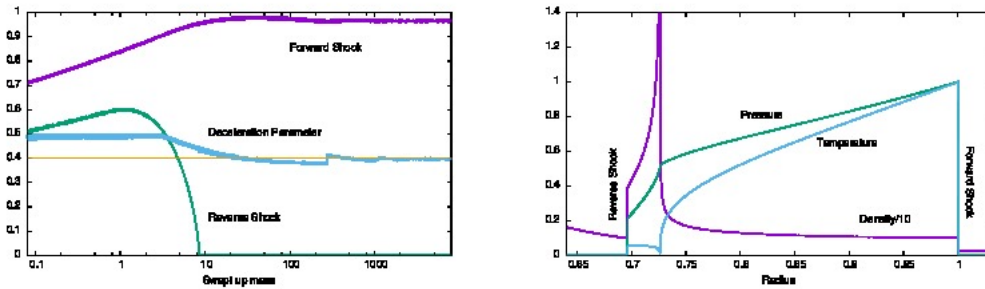


Fig. 8 Left: Shock locations and forward-shock expansion index m for the case $n = 6, s = 2$. Shock positions are scaled by $t^{0.4}$ (the Sedov value). Right: Profiles of density, temperature, and pressure during the self-similar phase for this calculation. (J. Blondin, private communication)

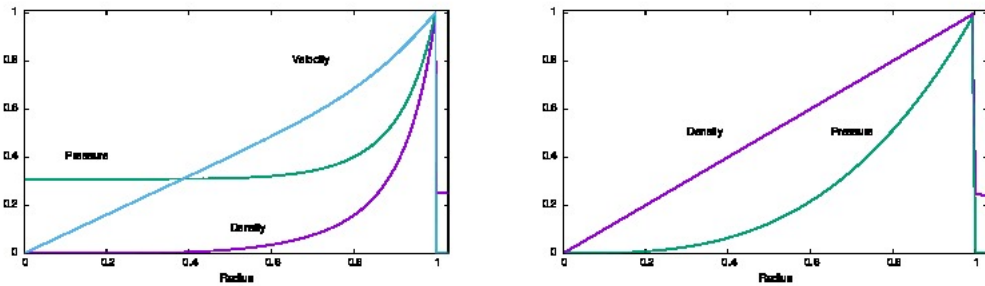


Fig. 9 Left: Sedov self-similar profiles of velocity, pressure, and density for a blast wave into uniform-density surroundings. Right: Sedov profiles for a blast wave into an r^{-2} density profile. Density and velocity profiles are identical in this case; both are linear with radius. (J. Blondin, private communication).

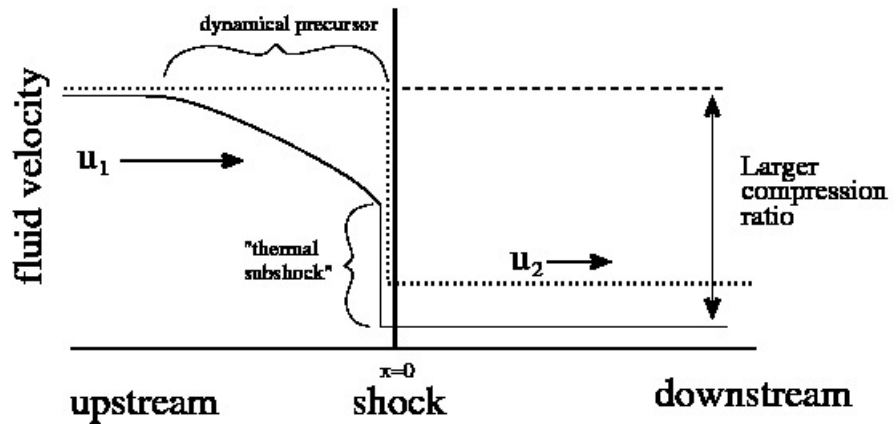


Fig. 10 Schematic of a cosmic-ray modified shock. In the shock frame, material enters from the left and is gradually decelerated by cosmic rays diffusing upstream in a "dynamical precursor" until a sharp drop in speed at the thermal subshock. The overall shock compression ratio can be considerably larger than in an unmodified shock.